Journal of Porous Materials
https://doi.org/10.1007/s10934-024-01703-8

Efficient synthesis of nanosized zeolite Y utilizing gradual heating: post-synthesis modification and their catalytic performance in propylene oligomerization

Cecilia Manrique[1] · Tatiana Botero[1] · Roger Solano[1,2] · Carlos Mendoza[1] · Adriana Echavarría-Isaza[1]

Abstract
Producing nanosized zeolites Y has been restricted to a Si/Al ratio lower than 2.0, requiring prolonged crystallization periods. This study employed temperature ramps during nucleation and crystallization to synthesize nanosized zeolites Y with a Si/Al ratio of 2.4, ranging from 47 to 100 nm, in just one day. Sequential post-synthesis desilication and dealumination treatments were used to modify the pore structure and acidity of the zeolites, leading to hierarchical zeolite formation. These modifications enhanced the structural stability and porosity of the zeolites while preserving their high crystallinity. Desilicated zeolites, unlike dealuminated ones, possessed straighter and more uniform mesoporous within their crystals, with diameters smaller than 5 nm. Additionally, successive desilication produced a greater number of intracrystalline mesoporous. The solids obtained from both processes exhibited porosity within the zeolite structure connected to the external surface, potentially improving the mass transfer limitations of the original zeolite due to the lack of mesoporous. Catalysts were prepared using modified nanozeolites for evaluation in the propylene oligomerization reaction. Catalysts based on dealuminated and desilicated nanosized zeolite Y showed high conversions above 20%, especially for dealuminated zeolites with conversions of 50%. Additionally, the catalysts demonstrated selectivity towards hydrocarbons in the C5-C7 range, suggesting better diffusion and access of propylene molecules to the active sites, favoring the formation of medium-sized hydrocarbon fractions. Conversely, the formation of longer hydrocarbon chains ($C12^+$) was not favored, possibly due to insufficient mesoporous for larger molecule diffusion and a distribution of acid sites that encourages the union of longer hydrocarbon chains.

Keywords Nanosized zeolite Y · Intraparticle and interparticle mesoporosity · Propylene oligomerization · Post-synthesis modification

1 Introduction

Zeolites are aluminosilicates with a microporous crystalline structure, which, due to their acidic properties and their shape selectivity, are used as catalysts in different industrial processes [1]–[4]. Zeolites are usually synthesized by the hydrothermal method under autogenous pressure. The study of the influence of the conditions of synthesis for obtaining zeolites is of great interest as itnot only allows for the improvement of their structural and chemical properties, but also reduces the costs associated with their synthesis. In addition, post-synthesis treatments have become a useful strategy for the design of catalysts to improve catalytic activity in many industrial processes. Among the most widely used zeolites on an industrial scale, zeolite Y is, to this day, one of the most important. Conventional zeolite Y has a faujasite-like crystal structure, with a Si/Al ratio of approximately 1.5. This zeolite typically has a lower surface area and lower thermal and hydrothermal stability compared to other materials [4–6]. To address these limitations, the synthesis of zeolite Y has focused on achieving Si/Al ratios greater than 1.5, shorter crystallization periods, and reduced crystal sizes. Reducing the crystal size aims to decrease diffusion limitations, thus increasing the surface area and consequently improving catalytic activity [7]–[9].

✉ Cecilia Manrique
alba.manrique@udea.edu.co

[1] Catalizadores y Adsorbentes, Instituto de Química, Facultad de Ciencias Exactas y Naturales, Universidad de Antioquia UdeA, Calle 70 No. 52-21, Medellín, Colombia

[2] Universidad EIA, Vía al aeropuerto José María Córdova Alto de Las Palmas, Kilómetro 2+200, Envigado, Colombia

Published online: 01 February 2025

The synthesis of zeolites of nanoscale sizes has received significant interest in recent times, and considerable advancements have been achieved in this area [10]–[14]. However, the synthesis of zeolites such as zeolite Y at the nanoscale represents a great challenge because its production at the nanoscale and with Si/Al ratios greater than 1.5 requires crystallization times greater than 5 days. Additionally, its small size also affects its hydrothermal stability, making it unsuitable for post-synthesis procedures like dealumination that would produce ultrastable zeolite Y (USY) because these treatments can destabilize the zeolite structure. Therefore, the search for more efficient and reproducible synthesis methods to produce nanosized zeolite Y with improved properties remains an active area of research. For zeolite Y, the synthesis of nanometric crystals has been reported mainly with the use of organic templates (structure-directing agents, SDAs), also used to obtain a zeolite Y with a high silicon-aluminum ratio [15–17]; however, the use of these templates increases the cost of synthesis and generates more pollutants. Most investigations on nanozeolites use the hydrothermal method for synthesis, and some researchers have concentrated on the effective parameters of green zeolite synthesis without structuring agents, such as crystallization time and temperature, aging, and gel composition. Temperature and time are important variables in zeolite synthesis, generating better control over nucleation and crystal growth rates [16]. For our study, precise control of these parameters is critical because it has been demonstrated in other porous material synthesis procedures that the heating rate up to the reaction temperature has a significant impact on the yield and products obtained. Furthermore, the heating rate affects the crystal's nucleation and growth, as well as its final size [18]. The synthesis temperature can be varied to control both the rate of crystal formation (nucleation) and the rate of growth. The rate at which the temperature changes between these two states is an important parameter to consider.

Zeolites have demonstrated their suitability for a range of applications, including catalysis, adsorption, and ion exchange. However, in catalysis, its microporous nature has demonstrated mass transfer problems because it limits the diffusion of reactants and products, both internally and between particles [19]. These limitations impact the efficiency of zeolites in terms of their activity, selectivity, and catalyst lifetime. These limitations could be addressed primarily through various means: (i) Decreasing the size of the crystal, (ii) including mesoporous inside the zeolite crystals, and (iii) incorporating mesoporous to a nanozeolite employing post-synthesis modifications, such as desilication and dealumination, to enhance the microporous characteristics of zeolites. These treatments improve both the physicochemical and catalytic characteristics of the zeolites, resulting in the creation of microporous materials that possess an additional structure with bigger pores (known as hierarchical zeolites). While post-synthesis treatments have been extensively studied in micrometric zeolites, there is less research on their impact on the structure and acidity of sub or nanometric-scale zeolites, which have potential use in catalysis [19].

The oligomerization reaction has remained one of the reactions of high interest and use at an industrial level. The main reasons for its importance are i) the oligomerization of low molecular weight olefins to produce higher molecular weight olefins and ii) olefin oligomerization as one of the basic steps in the methanol-to-olefin (MTO) process [20]. Generally, oligomerization reactions require acidic zeolites. Among the most used zeolites is the ZSM-5 zeolite (MFI structure), which has been shown to have unique physicochemical properties, limiting the formation of bulky polyaromatics that cause catalyst deactivation [21]. In addition, it exhibits good performance towards products from the fuel range. However, the industrial application of ZSM-5 has been hampered by its high deactivation rate and short lifetime due to mass transfer limitation in its tiny microporous. Currently, the study of olefin oligomerization on heterogeneous catalysts focuses mainly on increasing the activity and lifetime of the catalysts [22].

One of the zeolites that could be potentially useful in the oligomerization reaction is zeolite Y. Interest in this zeolite has grown due to its large pore size, which facilitates the diffusion of reactants and products, thus decreasing the rapid deactivation of the catalyst [23–25]. However, this feature is not enough on its own. It is necessary to increase the porosity and determine how the amount of aluminum in this zeolite can affect the acidity and, therefore, its behavior in the oligomerization reaction. Hence, this research intends to: a) highlight the obtention of a nano-scale zeolite Y with an environmentally friendly method, characterized by a high Si/Al ratio, temperature ramps during nucleation and crystallization and a short crystallization time, (b) determine its stability when subjected to treatments post-synthesis, such as dealumination and desilication, with the purpose of extracting aluminum or silicon to create a secondary porosity in the structure [26, 27], and (c) evaluate their behavior in the propylene oligomerization reaction to determine their selectivity and yield towards different hydrocarbon range.

2 Experimental

2.1 Synthesis

Faujasite (FAU-type zeolite) crystals were synthesized based on the method reported by Mendoza et al. [28] but using a different temperature during the nucleation and crystallization time. The composition of the precursor was as follow 20 mol SiO_2:0.7 mol Al_2O_3:8 mol Na_2O: 160 mol H_2O.

Experimental conditions such as aging time, crystallization temperature, and time were varied, as shown in Table 1. Sodium aluminate (53% Al_2O_3, 41% Na_2O, Sigma-Aldrich) was dissolved in deionized water, and then sodium hydroxide (99% Merck) was added. The mixture was stirred until complete dissolution and named Solution 1. In another recipient, sodium hydroxide was mixed with deionized water, and Ludox AM-30 (30% by weight of aqueous colloidal silica, Sigma-Aldrich) was subsequently added dropwise under constant stirring until complete dissolution. This solution was named Solution 2. Both solutions were left under stirring overnight to achieve a complete depolymerization of the species of aluminum and silicon. Subsequently, Solution 2 was added to Solution 1 under constant stirring, leaving two aging periods (δ1 and δ2) of 3–24 h at room temperature with an addition of fumed silica (99% Sigma-Aldrich) as an additional source of silicon between said periods. The obtained gel was transferred to teflon-lined autoclaves and treated hydrothermally under condition of temperature and time, as shown in Table 1. Since, the nucleation time and, in particular, the crystal growth rate are greatly affected by the heating method, in this work, a heating rate of 0.25 °C/min was used from room temperature until the first set point of temperature, and held at that temperature for desired time. Subsequently, the temperature was increased at the heating rate of 0.25 °C/min up to a second set point of temperature and held at that temperature for desired time. Then, the autoclaves were quenched, and the solid was recovered by filtration and washed with deionized water until the pH of the supernatant was neutral.

2.2 Post-synthesis treatments

2.2.1 Ion exchange

To obtain the nano zeolite in acid form, the sodium zeolite is refluxed at 60 °C for three hours with a 1 M aqueous solution of NH_4NO_3 (1 g of zeolite per 50 ml of aqueous solution). The solid was then washed with deionized water and dried at 100 °C overnight. The resulting material was calcined at 500 ºC for 2 h and named HY.

2.2.2 Dealumination

The nanosized zeolite Y was subjected to a sequential dealumination process. First, the sodium zeolite was initially transformed to its ammoniacal form through two ionic exchanges of 3 h at 60 °C, using an aqueous solution of NH_4NO_3 1 M (1 g of zeolite per 50 mL of aqueous solution). Subsequently, the solid was washed with deionized water and dried at 100 °C overnight. The zeolite in its ammoniacal form was subjected to dealumination by treatment in water vapor (bath temperature of 80 °C) at 700 °C for 3 h, under air flow 50 ml /min. The obtained solid was again put

Table 1 Structural and chemical composition of the synthesized zeolites

Sample	δ1 (h)	δ2 (h)	Crystallization conditions				Phase	Crystallinity[a] (%)	Si/Al[b] framework	Crystal size [c] (nm)
			Tc_1 °C	tc_1 h	Tc_2 °C	tc_2 h				
CBV 300							FAU	100	2.5	172
NaY0	24	24	100	18	–	–	Amorpho	–	–	–
NaY1	24	24	60	4	100	14	FAU	83.4	2.2	58
NaY2	24	24	60	6	100	12	FAU	85.3	2.2	47
NaY3	3	3	60	4	100	14	Amorpho	–	–	–
NaY4	3	3	60	6	100	12	Amorpho	–	–	–
NaY5	3	3	60	4	100	20	Amorpho	–	–	–
NaY6	3	3	60	6	100	18	Amorpho	–	–	–
NaY7	3	3	80	12	100	24	Amorpho	–	–	–
NaY8	3	3	100	24	–	–	Amorpho	–	–	–
NaY9	3	3	85	4	105	20	Amorpho	–	–	–
NaY10	3	3	100	36	–	–	Amorpho	–	–	–
NaY11	3	3	80	6	100	30	Amorpho	–	–	–
NaY12	6	6	80	12	100	24	FAU	82.6	2.4	100
NaY13	6	6	100	36	–	–	FAU- Amorpho	37.9	NA	NA
NaY14	12	12	80	12	100	24	FAU	92.9	2.3	83
NaY15	12	12	100	36	–	–	FAU	87.6	2.3	80

δ aging period (h). *Tc* Crystallization temperature, *tc* Crystallization time. [a]Determined by X ray diffraction (XRD). [b]Framework Si/Al ratio from XRD. [c]Determined using the Scherrer equation

through 1.0 M NH_4NO_3 solution by 3 h at room temperature and dealuminated again. This process was repeated four times, and the solids obtained in each stage were named HYS1, HYS2, HYS3, and HYS4.

2.2.3 Desilication

For the desilication, 1 g nanosized zeolite Y per 40 ml of a NaOH solution 2 M was stirred in reflux during 1 h at 60 ºC. The solid obtained was recovered by centrifugation, followed by washing with deionized water until pH = 7 and drying at 100 °C overnight. This process was repeated four times, and the solids obtained in each stage were named NaYL1, NaYL2, NaYL3, and NaYL4. Then, the zeolites were treated by ion exchange in 1 M NH_4NO_3 solution at 60 °C for 3 h with ratio of 1 g zeolite/50 mL solution. After ion exchange, the zeolites were converted to proton-type zeolites by calcination at 500 °C for 1 h in air flow (50 ml/min). The final samples were tagged HYL1, HYL2, HYL3, and HYL4.

2.3 Preparation of the catalysts

Catalysts were prepared as follows. A mechanical mixture of dealuminated or desilicated zeolite in its acid form (30 wt%) and alumina (Versal 250 pseudoboehmite alumina, surface area of 320 m^2/g) were peptized using a 1 wt% HNO_3 solution as peptizing agent. The dough obtained was extruded in cylindrical shape, and the resulting material was dried at 100 °C and calcined at 500 °C for 2 h.

2.4 Oligomerization catalytic tests

The catalytic tests were carried out in a fixed bed reaction system. First, the catalyst was pre-treated at 150 °C for 30 min with a total N_2 flow of 50 ml/min. Afterwards, reactant mixture 5% propene/N_2 at 30 ml/min, 2760 kPa and weight hourly space velocity (WHSV) of 1 h^{-1} was exposed. The reaction products were analyzed each hour during 4 h by gas chromatography with an FID detector and a DB1 column until the activity remained constant. Then, the temperature was increased within the range of 150–300 °C every 50 °C.

2.5 Characterization methods

Zeolites were characterized by XRD at room temperature in a PANalytical Empyrean diffractometer with a CoKα radiation (λ = 1.7903 Å) operating at 45 kV and 40 mA. Samples were analyzed in the 5–50º (2θ) range with a step size of 0.04º. The average crystallite size from XRD for the original zeolite was estimated by the Scherrer equation. The LaB_6 was used to determine the broadening of the instrumentation [26]. The ASTM D3906-03 method was used to calculate the crystallinity of the original and modified zeolites, the sum of the areas of the six most intense peaks in the interval 14–35° 2θ of the XRD (S_x) was divided by the sum of the areas of the six most intense peaks the zeolite CBV 300 (S_{ref}) [29]. The Si/Al ratio of the crystalline lattice of the synthesized zeolites was calculated by the Breck and Flanigen equation where the cell parameter (a_o) was found by a Le Bail fit [30, 31]. Elemental analysis was determined by atomic absorption spectroscopy on a Thermo Scientific iCE 3000 equipment. All samples were treated with hydrofluoric acid (40% PanReac) to completely dissolve it.

Nitrogen sorption measurements of zeolites were performed with a Micromeritics ASAP 2020 gas sorption system at -196 ºC. Prior to the measurements, the samples were degassed under high vacuum conditions for 8 h at 350 °C. The apparent specific surface area (S_{BET}) and micropore volume (V_{micro}) were calculated using the Brunauer–Emmet–Teller (BET) and t-plot methods, respectively. Pore size distributions were obtained using the DFT method.

Acid properties of zeolites were determined by temperature programmed desorption of ammonia NH_3-TPD and isopropylamine (IPam-TPD). NH_3-TPD experiments were carried out in Micromeritics ChemiSorb 2720 equipment with a thermal conductivity detector (TCD). Prior to the measurements, about 0.2 ± 0.01 g of zeolite was placed in a quartz reactor and then heated up to 150 °C for one hour. Subsequently, the temperature was increased at 400º C with a temperature ramp of 10 °C/min under N_2 flow (30 ml/min), and held for 1 h. After cooling down to 150 °C, ammonia adsorption took place for 5 min at 5 ml /min. Physically adsorbed ammonia was removed with N_2 flow for 1 h. Ammonia desorption was performed at a rate of 10 °C/min, starting at 100 °C and reaching up to 550 °C under He flow (30 ml/min).

To determine the amount of Brønsted acid sites, temperature programmed desorption of isopropylamine measurements were performed. Experiments were carried out in a Micromeritics ChemiSorb 2720 equipment coupled to a mass spectrometer (MKS Cirrus 2). Here, 0.1 ± 0.01 g of zeolite was placed in a quartz reactor and then heated to 200 °C using a temperature ramp of 10 °C/min under a He flow of 25 ml/min for one hour. After cooling down to 100 °C, isopropylamine adsorption took place through small pulses. Full saturation was verified, and physically adsorbed isopropylamine was removed by flushing the sample with He flow for 30 min. Isopropylamine desorption was performed at a heating rate of 10 °C/min, starting from 100 °C and reaching up to 600 °C under He flow (25 ml/min), followed by a one-hour isothermal step.

TEM images of the zeolite particles were taken in a FEI Tecnai G2 F20 microscope operating at 200 kV. Prior to measurements, the samples were suspended in ethanol,

sonicated for 30 min, and placed over a carbon coated holey Cu microgrid.

The surface chemical information was determined by X-ray photoelectron spectroscopy (XPS, SPECS) with a PHOIBOS 150 1D-DLD analyzer and monochromatic Al Kα radiation (1487 eV) operated at 10W. The XPS spectra were recorded with a pass energy of 90 eV and step size of 0.01 eV for general spectra and a pass energy of 20 eV and step size of 0.05 eV for high-resolution spectra. Adventitious C1s core level line was selected as reference to calibrate the energy scale. The spectra were analyzed by using a Gaussian – Lorentzian blend (GL 20–30%) and a Shirley type background subtraction.

3 Results and discussion

3.1 Characterization of synthesized zeolites Y

The XRD results for the synthesized samples are presented in Table 1 and Fig. 1. All zeolites crystalline (NaY1, NaY2, NaY12, NaY14, and NaY15) have a relative crystallinity greater than 80%. The Si/Al ratio in the framework for these zeolites was found to be greater than 2.1 and have a primary crystal size less than or equal to 100 nm. The initial synthesis conditions for sample NaY0 did not favor the formation of the FAU crystalline phase. It is well known that the rate of nucleation and growth of the crystal in zeolites is determined by different synthesis parameters, such as gel composition and crystallization time and temperature [32].

With the purpose of favoring the formation of crystals with FAU structure, two different crystallization temperatures and times were employed in each synthesis using a heating ramp of 0.25 °C/min. For samples with an aging period of 24 h (samples NaY1 and NaY2, Table 1), the formation of the FAU crystalline phase was possible. A low crystallization temperature at short times followed by a high crystallization temperature with long times proved to be a viable method for the formation of the FAU-type structure. The NaY1 sample (Tc_1 of 60 °C and tc_1 of 4 h) favored the formation of a zeolite Y-type structure with a high crystallinity (83.4%) and with nanometric-sized crystals (58 nm). However, the NaY2 sample (Tc_1 of 60 °C and tc_1 of 6 h) presented a higher relative crystallinity (85.3) and a smaller primary crystal size (47 nm) than NaY1. This result indicates that an increase in the crystallization time tc1 could favor the obtention of smaller crystals. On the other hand, under identical crystallization conditions applied to samples NaY1 and NaY2, reducing the aging time to 3 h to produce samples NaY3 and NaY4, it is not possible to obtain the crystalline phase; that is, the aging time of 3 h is not sufficient for the formation of nuclei under these conditions. When using an aging time of 3 h (samples NaY3-11), it is observed that an increase in temperature and crystallization time favors the appearance of peaks that correspond to the FAU crystalline phase. However, the percentage of relative crystallinity for these samples is very low and the amorphous content predominates. On the other hand, extending the aging period leads to the generation of zeolites with enhanced relative crystallinity.

This enhancement becomes noticeable when prolonging the aging period in samples NaY7 to acquire sample NaY14, and in sample NaY10 to obtain sample NaY15. The aging period was increased from 3 to 12 h in both instances. As a result, samples NaY14 and NaY15 demonstrate the highest relative crystallinity compared to samples NaY7 and NaY10, which were synthesized under identical crystallization conditions but with a different aging time. In addition, a decrease in the size of the primary crystal is observed with increasing aging time, which is associated with nucleation favored by longer aging times.

However, if the synthesis is conducted without a secondary crystallization temperature, and the first crystallization period and temperature are increased as compensation, a reduction in relative crystallinity is observed mainly when using a short aging time. This can be seen when contrasting samples NaY12 and NaY13 of 6 h of aging, and samples NaY14 and NaY15 of 12 h of aging. NaY13 shows amorphous presence and low relative crystallinity compared to NaY12, while NaY15, although not showing amorphous characteristics, shows a decreased relative crystallinity compared to NaY14. This outcome suggests that the gradual temperature increase achieved through a secondary crystallization process promotes an adequate growth rate for zeolite nuclei, especially at lower temperatures.

Materials with high relative crystallinity and nanoscale-sized crystals with dimensions less than 100 nm or in the submicron range, equal to or larger than 100 nm, have been obtained according to the defined synthesis conditions. As the particle size of zeolite is reduced to the submicron or nanometer scale, the diffusion limitation of reactants and products decreases, consequently enhancing mass transport through the zeolite channels [33, 34]. Nevertheless, it has been reported that post-synthesis treatments may cause structural damage to reduced-sized zeolites, particularly at the nano scale [19]. Therefore, to implement the procedures described in the methodology, it was determined that sample NaY12 possesses a Si/Al ratio of 2.4, a primary crystal size of 100 nm, and a relative crystallinity that exceeds 80%, in contrast to other samples with smaller primary crystal sizes. Due to the possibility of structural degradation in smaller samples, sample NaY12 is more suitable for post-synthesis treatments. Additionally, sample NaY12 was obtained under appropriate synthesis time and temperature conditions.

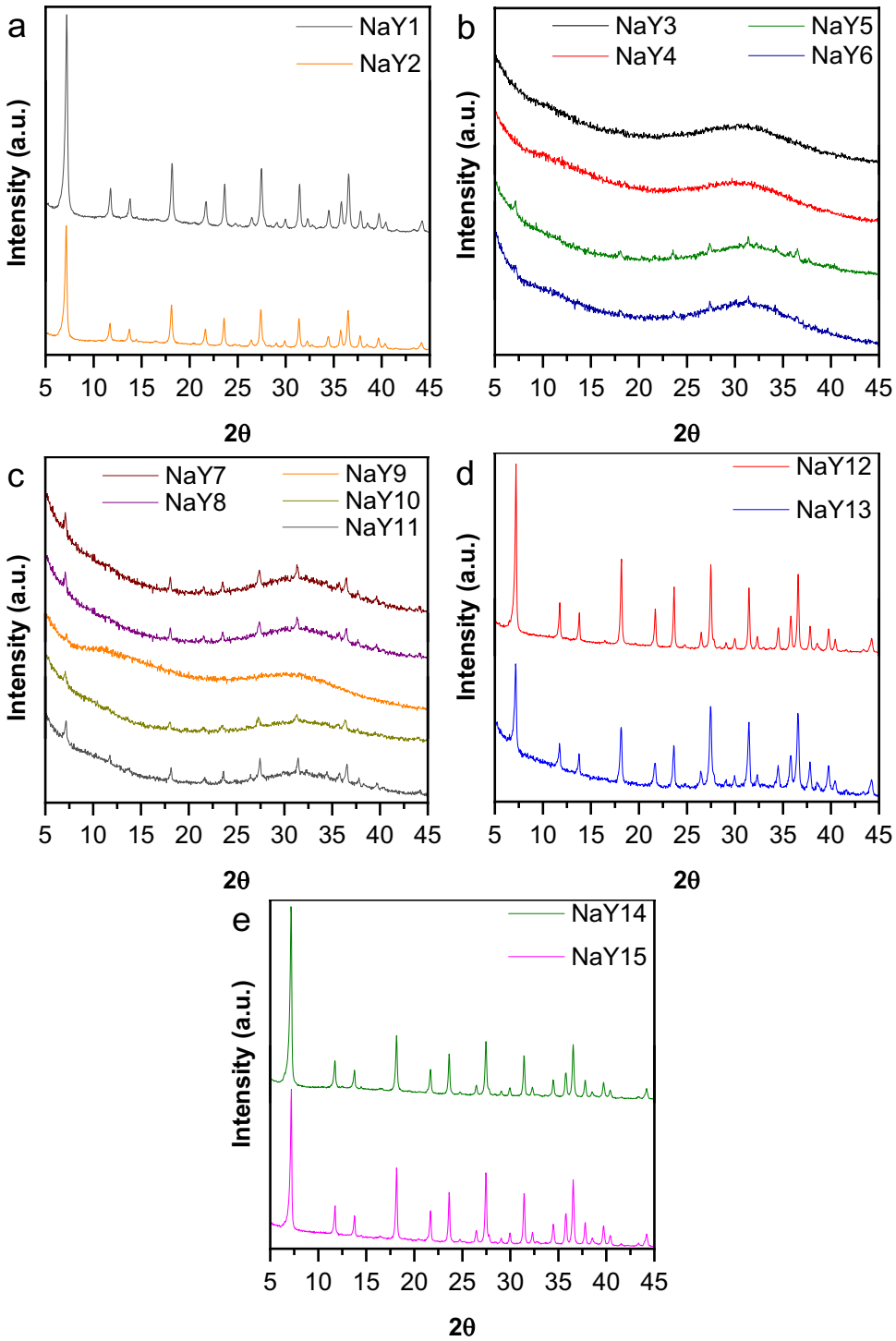

Fig. 1 XRD patterns of zeolites NaY. **a** Aging 24 h **b** Aging 3 h and Tc1 < 80 °C **c** Aging 3 h and Tc1 > 80 °C **d** Aging 6 h **e** Aging 12

3.2 Structural characterization of modified zeolites Y

Dealumination of the zeolite NaY12 (hereafter referred to as NaY) resulted in a shift towards greater 2θ values in diffractograms (Fig. 2) as the number of steaming treatments increased. The shift was associated with an increase in the Si/Al ratio in the structure, as seen in Table 2. After the first process of steaming (HYS1), zeolite Y with a Si/Al ratio greater than 3.0 was obtained, which is a favorable result because this ratio cannot be directly achieved during synthesis. The repetition of the steaming treatment has a direct effect on the Si/Al ratio, which in turn affects the acidic properties of materials. In this work, a zeolite with a Si/Al ratio of 10.4 (designated as HYS4) was effectively obtained following four consecutive treatments at 700 °C

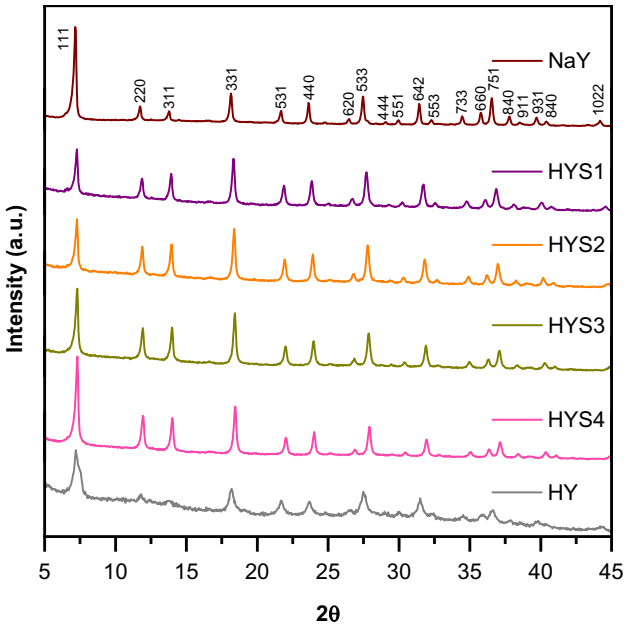

Fig. 2 XRD patterns of zeolites dealuminated

Table 2 Results of XRD analysis of dealuminated zeolites Y

Sample	Crystallinity[a] (%)	Si/Al[b] framework	Crystal size[c] (nm)	Si/Al[d] bulk
CBV 300	100	2.5	171.8	2.5
NaY	82.6	2.4	100	2.4
HY	63.5	3.6	70.0	2.5
HYS1	74.5	3.8	42.2	2.6
HYS2	76.4	5.8	59.2	2.6
HYS3	81.6	7.9	48.0	2.7
HYS4	85.1	10.4	46.7	2.7

[a]Determined by X ray diffraction (XRD) [b]Framework Si/Al ratio from XRD [c]Determined using the Scherrer equation [d]Bulk Si/Al ratio from AAS

Table 3 Results of analysis of XRD zeolite Y After alkaline treatment

Sample	Phase	Cristallinity[a] (%)	Si/Al[b] bulk
CBV 300	FAU	100	2.5
NaY	FAU	82.6	2.4
HY	FAU	63.5	2.5
HYL1	FAU- amorpho	38.8	2.5
HYL2	FAU- amorpho	33.8	2.2
HYL3	FAU- amorpho	30.5	2.0
HYL4	FAU- amorpho	20.0	2.0

[a]Determined by X ray diffraction (XRD). [b]Bulk Si/Al ratio from AA

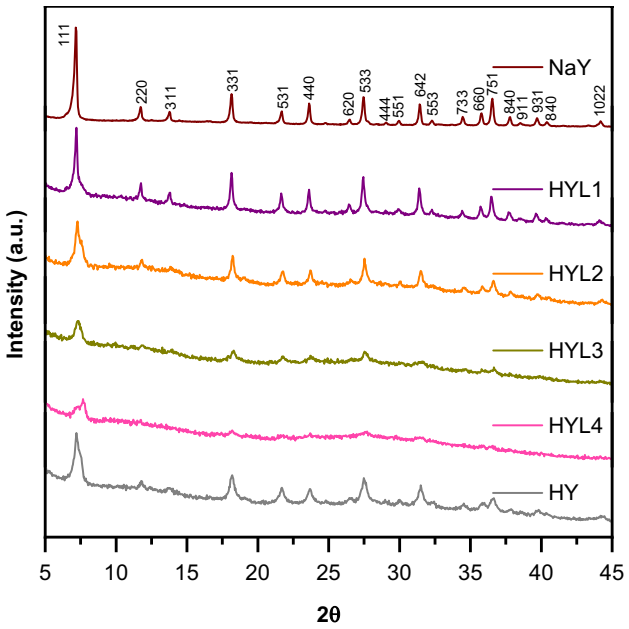

Fig. 3 XRD patterns of zeolites after desilication

for three hours each. In Table 2, it is seen that crystallinity increases as more steaming process is applied to the material (HYS1→HYS2→HYS3→HYS4) due to the reconstruction of lattice zeolite as reported in the literature [11]. In addition, the dealuminated zeolites exhibit a smaller main crystal size compared to pristine zeolite NaY due to crystal fragmentation during aluminum extraction from the framework. Nevertheless, it is important to note that the bulk Si/Al ratios remain constant for all dealuminated Y zeolites, as shown in Table 2, due to the extraframework Al species remain in the sample and are not leached.

On the other hand, nanosized zeolite Y was also desilicated successively with NaOH. Table 3 shows the depletion of Si/Al ratio due to the leaching process, as silicon is dissolved. Figure 3 depicts the X-ray diffraction patterns of desilicated zeolites, demonstrating that the crystalline FAU phase is preserved. However, the relative crystallinity of the four solids shows a drop of more than 50% after following the first treatment (Table 3). These observations suggest that the desilication conditions were excessively aggressive for the nanosized zeolites. The high alkalinity likely causes non-selective silicon dissolution, leading to a loss of crystallinity in the materials.

The particle size and presence of mesoporosity in HY, HYS1, HYS2, HYL1, and HYL2 zeolites has been evaluated by transmission electron microscopy (TEM), as depicted in Fig. 4. The average crystalline size of the zeolite HY ranges from 80 to 100 nm, which aligns well with the calculations made using the Scherrer equation for the starting zeolite NaY (see Table 1, sample NaY12). The post-synthesis

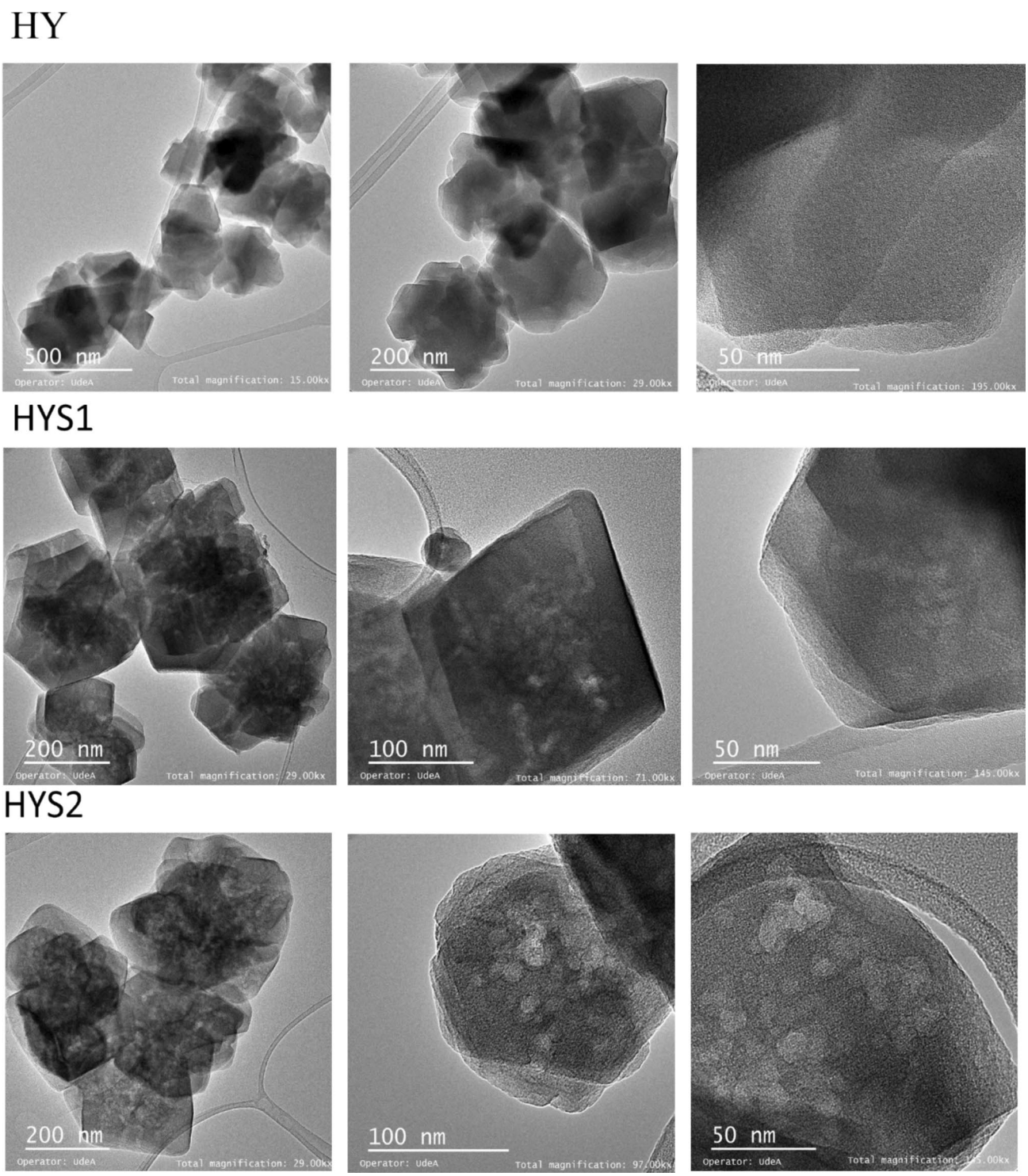

Fig. 4 TEM images of zeolites Y

modifications, such as desilication and dealumination, have affected the edges of the zeolites, resulting in a decrease in their crystallinity, mainly in the desilication process. Although these modifications are beneficial for introducing mesoporous, they compromise the structural integrity of zeolites due to the tensions and deformations they create. In the dealuminated samples (HYS1 and HYS2), the average size of the mesoporous is slightly larger than in the desilicated samples (HYL1 and HYL2). The shapes of mesoporous in dealuminated zeolites are spherical pores

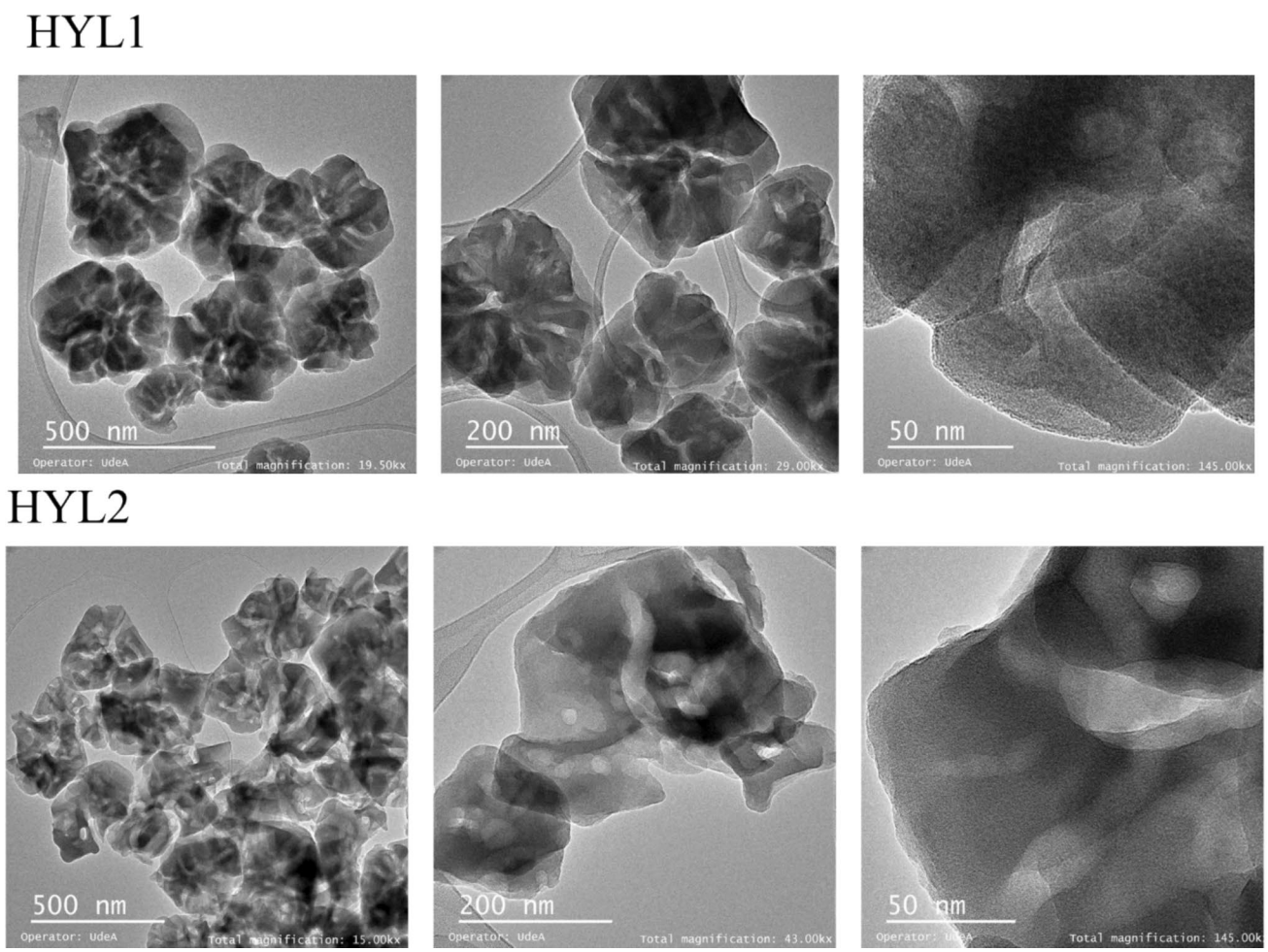

Fig. 4 (continued)

interconnected with the particle surface. Furthermore, the mesoporous in the HYS2 zeolite exhibit larger sizes compared to HYS1, suggesting a progressive increase in pore size during the dealumination process. This treatment also significantly affects the crystals morphology and size since the crystal size of HYS1 and HYS2 zeolites decreased. These results are consistent with previous studies that demonstrate that dealumination can alter the crystalline structure of zeolites and increase the size of mesoporous [35]. On the other hand, desilication decreases the size of the zeolite NaY crystal to approximately 80 nm through treatment with NaOH. This process causes a decrease in the crystalline structure due to the action of HO- anions, both on the surface and inside the zeolite. The TEM images also reveal that the desilicated zeolites, unlike dealuminated ones, possess straighter and more uniform mesoporous within their crystals, with pore diameters smaller than 5 nm. Furthermore, the successive desilication procedure yields a higher quantity of intracrystalline mesoporous. The solids obtained in both processes showed porosity within the zeolite structure, connected to the external surface. Therefore, they could contribute to improving the mass transfer drawbacks that the original zeolite presents by not having mesoporous.

Table 4 displays the Si/Al ratio on the external surface, which was established by calculating the atomic percentage using the area under the curve of the Si 2p and Al 2p signals observed in the XPS spectra. To assess the diversity of the

Table 4 Si/Al ratio determined by XRD, AAS and XPS for nanosized zeolites Y obtained by dealumination and desilication

Sample	$Si/Al_{(fram)}$ [a]	$Si/Al_{(bulk)}$ [b]	$Si/Al_{(surf)}$ [c]	$Si/Al_{surf}/Si/Al_{bulk}$
HY	2.5	2.5	4.0	1.6
HYS1	3.8	2.6	3.0	1.2
HYS2	5.8	2.6	2.8	1.1
HYL1	-	2.3	1.7	0.8
HYL2	-	2.1	1.4	0.6

[a]Framework Si/Al ratio from XRD. [b]Bulk Si/Al ratio from AAS. [c]Surface Si/Al ratio from XPS

synthesized zeolites, this Si/Al ratio of the zeolites was compared to the Si/Al ratio of the framework and the Si/Al ratio in the bulk. The surface Si/Al ratio in the nanosized zeolite HY is higher compared with the bulk Si/Al and framework Si/Al ratio, suggesting a heterogeneous composition where the interior of the zeolite contains a larger concentration of aluminum. This result is due to the synthesis conditions used since the production of nanoscale zeolite with a low Si/Al ratio is facilitated by creating aluminum-rich nuclei during the aging phase, and then coating on the surface with the silica that is added afterwards.

When the nanozeolite is treated with a dealumination procedure (HYS1) in its ammoniacal form, the surface Si/Al ratio is slightly higher than the bulk ratio but lower than the framework ratio. This result suggests that the sample has a minimal concentration of aluminum on its surface. The decrease in aluminum (Al) on the surface of the zeolite can be attributed to the transformation of Al species found on the outer surface of the zeolite crystals into extra-framework aluminum (EFA) species [36]. When sequential dealumination is carried out (HYS1 → NH4Y12 → HYS2), surface Si/Al to bulk Si/Al ratio changes from 1.17 to 1.07. This suggests that twice vaporization marginally reduces the amount of Al in the HYS1 sample. The proximity of the Si/Al ratio to 1.0 indicates that the sample has a uniform composition.

During the desilication process of NaY zeolite, the use of a highly concentrated NaOH solution resulted in significant dissolution of the zeolite structure, causing a substantial extraction of a large amount of Si species from the outer surface to the inner pores. During the sequential desilication process (NaYL1 → NaYL2) and the subsequent ion exchange to obtain HYL2, surface Si/Al to bulk Si/Al ratio changes from 0.8 to 0.6. This change causes a decreased dissolution of the Si species and a slight reduction in its crystallinity compared to the HYL1 zeolite, as shown in Table 4 and Fig. 3.

3.3 Textural characterization of modified zeolites Y

Figure 5 shows the N_2 adsorption/desorption isotherms of different nanosized zeolites. The corresponding textural properties are listed in Table 5. Zeolites NaY, HY, and desilicated (HYL1 and HYL2) exhibit a classic type I isotherm,

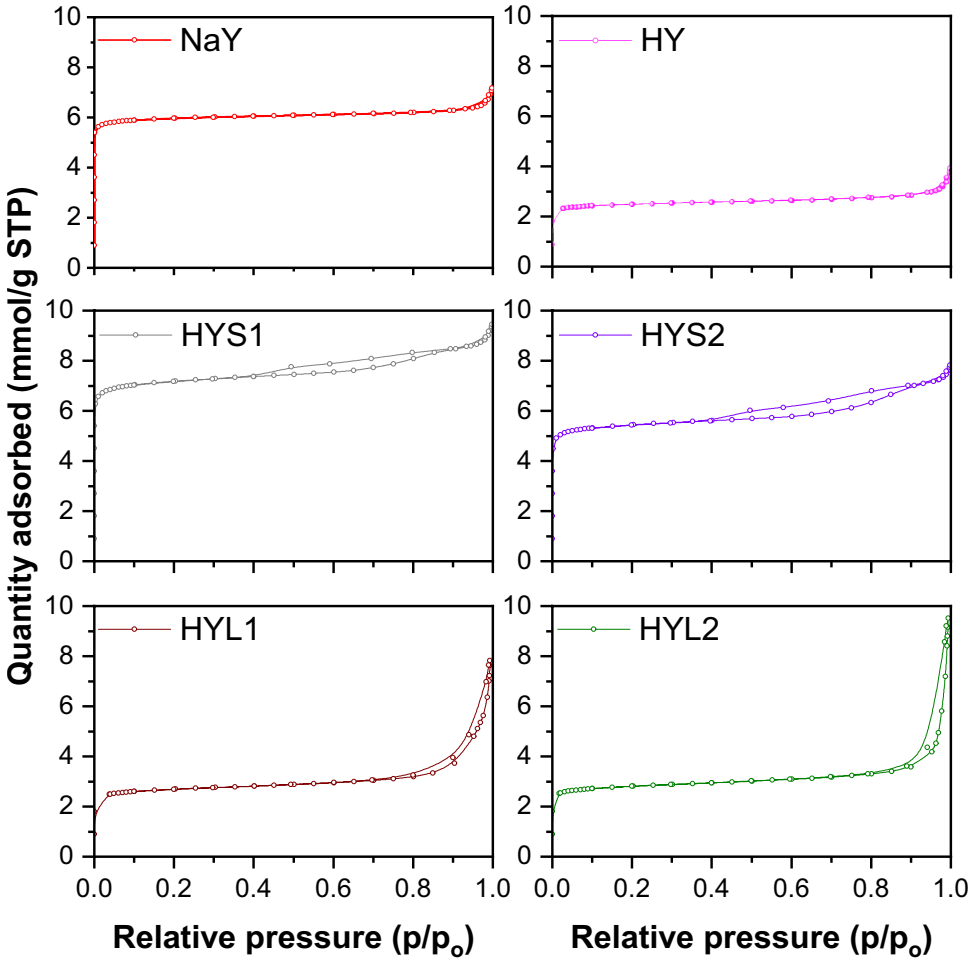

Fig. 5 N_2-adsorption/desorption isotherms of the parent NaY and modified zeolites

Table 5 Textural properties of zeolites obtained from the N_2 sorption isotherms

Sample	S_{BET} [a]	S_{micro} [b]	S_{ext} [c]	V_{total} [d]	V_{micro} [e]	V_{meso} [f]
NaY	546	512	34	0.25	0.19	0.05
HY	220	189	31	0.14	0.07	0.06
HYS1	645	578	67	0.33	0.22	0.11
HYS2	487	430	57	0.27	0.16	0.11
HYL1	234	192	42	0.27	0.07	0.20
HYL2	245	200	44	0.33	0.08	0.25

[a]BET specific surface area (m^2/g). [b]t-plot micropore area (m^2/g). [c]t-plot external surface area (m^2/g). [d]Total pore volume (cm^3/g). [e]t-plot micropore volume (cm^3/g). [f]Mesopore volume, V_{total}–V_{micro} (cm^3/g)

with a steep rise in uptake at low relative P/Po pressure and a flat curve afterwards, which is typical for microporous materials. A significant difference exists between the sodium sample and the exchanged sample; obviously, ion exchange extensively affects nanozeolites. All the textural properties decrease to less than half, which indicates that this treatment destroys a large part of the nanozeolite structures, possibly due to the size of the crystals which would allow a dissolution of the samples. Dealuminated zeolites shows an isotherm that would be a mixture between a type 1 and a small contribution of type 4 isotherm, indicating that microporosity is maintained with a few mesoporous due to the increase in the amount adsorbed throughout the relative pressure change. Additionally, large hysteresis loops type H4 are observed after a relative pressure of 0.4, indicating the presence of mesoporous with a wide pore size distribution, which may be due to the extraction of aluminum from the zeolite lattice. Desilicated zeolites show an increase in the adsorption of N_2 from a relative pressure of 0.8 characteristic of capillary condensation in open mesoporous or macroporous obtained by filling the spaces between particles. These samples present a H1 type hysteresis loop that is related to mesoporous due to interparticle voids, probably because of their smaller size, as observed by XRD and electron microscopy.

Table 5 shows the results of the textural properties of all zeolites obtained from the N_2 adsorption/desorption isotherms. The dealumination treatment does not considerably affect the textural properties of the samples; even a single treatment improves these properties (HYS1 gain of 20% and HYS2 loss of 10%). The desilication process changed the BET specific surface area, about 60% of the area of the original zeolite. The reduction in area must be related to the partial destruction of the structure, considering that these materials presented the lowest crystallinity (Table 2). In general, modified samples showed a reduction of area and volume of microporous related to zeolite NaY but an increase in mesoporous, as expected. Again, dealumination treatment yielded a larger volume of mesoporous than the original zeolite.

Figure 6 shows the pore size distribution by DFT for all samples. The original zeolite has a size distribution centered at approximately 0.6 nm, as expected for a microporous zeolite. When performing the exchange to this zeolite, it is observed that the number of pores decreases substantially and shifts slightly to higher pore size values. Additionally, a second type of pore would be generated at greater pore widths, but in very small amounts, corroborating the previously observed destruction of the zeolite structure after this treatment. For dealumination and desilication treatments,

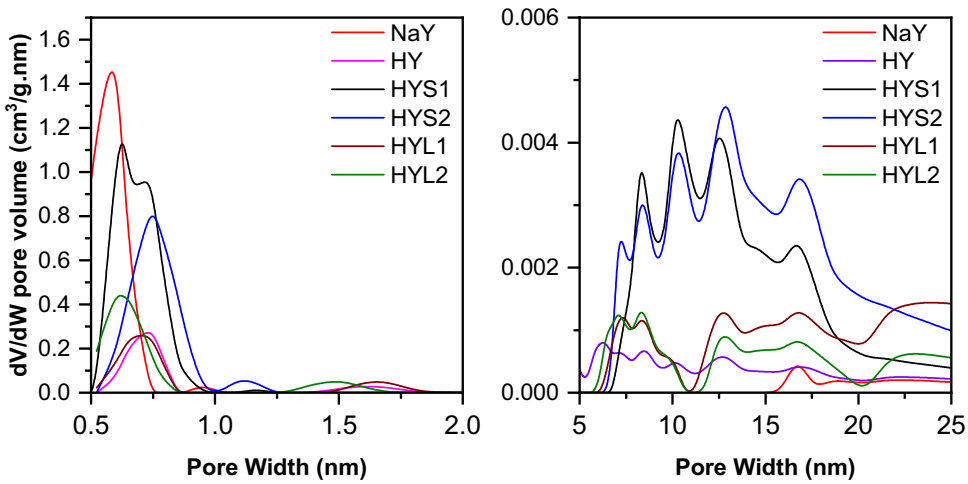

Fig. 6 Pore size distribution of the parent NaY and modified zeolites

it is observed that the main pore size distribution shifts to higher values around 0.8 nm, and, additionally, different wider pore sizes are generated. For the desilicated zeolites, a small number of pores is observed around 1.5 nm and a wide distribution from approximately 20 nm. For dealuminated zeolites, a considerable increase in pores is observed in the range of 5 to 20 nm, indicating that dealumination generates larger pores.

3.4 Acidity characterization of modified zeolites Y

Figure 7 presents temperature-programmed desorption of ammonia (NH3-TPD) profiles of Y zeolites. These profiles were arbitrarily deconvoluted into two desorption peaks, corresponding to the weak and strong acidic sites on the pristine and modified Y zeolites. Table 6 presents the results of surface acidity characterized by temperature programmed desorption of ammonia (NH3-TPD) and isopropylamine. The desilicated solids maintain the total acidity with respect to the mother zeolite, while the acidity of the dealuminated sample decreases by a significant amount, indicating that the desalination treatment affected the surface acidity to a greater extent due to the extraction of aluminum from the zeolite lattice. Additionally, the post-synthesis treatments generated an additional peak in the samples at low temperatures, presenting three peaks: the first around 180° C weak acid sites, the second around 220 °C intermediate acid sites, and the third around 390 °C strong acid sites. When observing the relation of total acid sites with the original sample (TAn), the dealuminated samples lose more than 50% of the acid sites, while the desilicated samples lose around 15%, confirming that the dealumination treatment is more severe than that of desilication. The ratio of strong acid sites to intermediate acid sites (SS/IS) increases with the dealumination treatment by around 20% and decreases with the desilication treatment. When performing the dealumination treatment only once, it is observed that the Brønsted acid sites increase, while the rest of the treatments decrease them considerably.

3.5 Insights from studying catalysts in oligomerization

Catalysts obtained from modified and unmodified nanometric zeolites Y were evaluated in the reaction of propylene oligomerization. As the zeolite-alumina ratio was the same for preparing all catalysts, the catalytic activity will be directly related to the properties of zeolites. For comparison purposes, a catalyst was evaluated using a commercial CBV 400 zeolite Y, the 4.0 Si/Al acid zeolite from CBV300 steaming. The effect of the time on stream in conversion and selectivity over nanosized zeolite Y-based catalysts is shown in Figure S1. Catalysts showed high catalytic activity at 150 °C, especially in the first hours of the reaction until reaching a constant activity. The catalysts derived from dealumination processes exhibit a higher conversion during 4 h of reaction in comparison to the original nanosized zeolite Y (HY) and commercial CBV 400. The higher conversion primarily due to the modification of the acid sites and the formation of interparticle mesoporosity, as observed in the TEM micrographs and as reported in other studies [37, 38]. The transport of propylene molecules through the pores of the zeolite is facilitated by the structural modifications carried out by the post-treatments. The generation of mesoporosity provides access to previously inaccessible Brønsted acid sites and, therefore, significantly improves catalytic activity. Nevertheless, the modified catalysts exhibit a lower selectivity towards hydrocarbons, including C_3-C_4, C_5-C_7, C_8-C_{12}, and C_{12}^+, compared to CBV 400, during the 4 h of reaction. This decrease in selectivity suggests that the formation of intraparticle mesoporous results in an excessive cracking of hydrocarbon molecules, which in turn leads to a broader spectra of smaller hydrocarbons. The nanosized zeolite HYS2 does not substantially improve selectivity towards specific hydrocarbon fractions despite the improvement in conversion. Therefore, improving mesoporosity and modifying acid strength to enhance conversion rates may also induce undesirable side effects, such as excessive fragmentation, which could affect selectivity for larger products such as C_{12}^+.

To compare the catalysts' activities, it is suitable to use the dependence of conversion on the process temperature. After observing stability in the catalytic activity, the temperature was then raised in 50 °C increments up to 300 °C. As can be seen in Fig. 8, in the same temperature range, there is an increase in the conversion when the temperature is increased. For the original zeolite and the desilicated zeolites (HYL1 and HYL2), the increase in conversion is linear with the temperature, showing initially a higher activity in zeolite HYL2; however, at 300 °C both desilicated zeolites present a conversion of 20%. On the other hand, the dealuminated zeolites increase their conversion up to 200 °C and remain stable for a conversion of 37% and 47% for the zeolites HYS1 and HYS2, respectively. The catalyst conversion follows the following order HYS2 > HYS1 > CVB400 > HYL2 > HL1 > HY. This order is linear with the relationship found between microporous area and Bronsted acid sites (Table 6 and Figure S2), wich indicates that the increase in the conversion over the reaction temperature could be associated mainly with the distribution of Bronsted acid sites, preferentially over zeolite microporous.

Catalysts based on dealuminated and desilicated nanosized zeolite Y have demonstrated high selectivity towards hydrocarbons in the C_5–C_7 range (Fig. 9), which suggests that better diffusion and access of propylene molecules to the active sites has been achieved, favoring the formation of

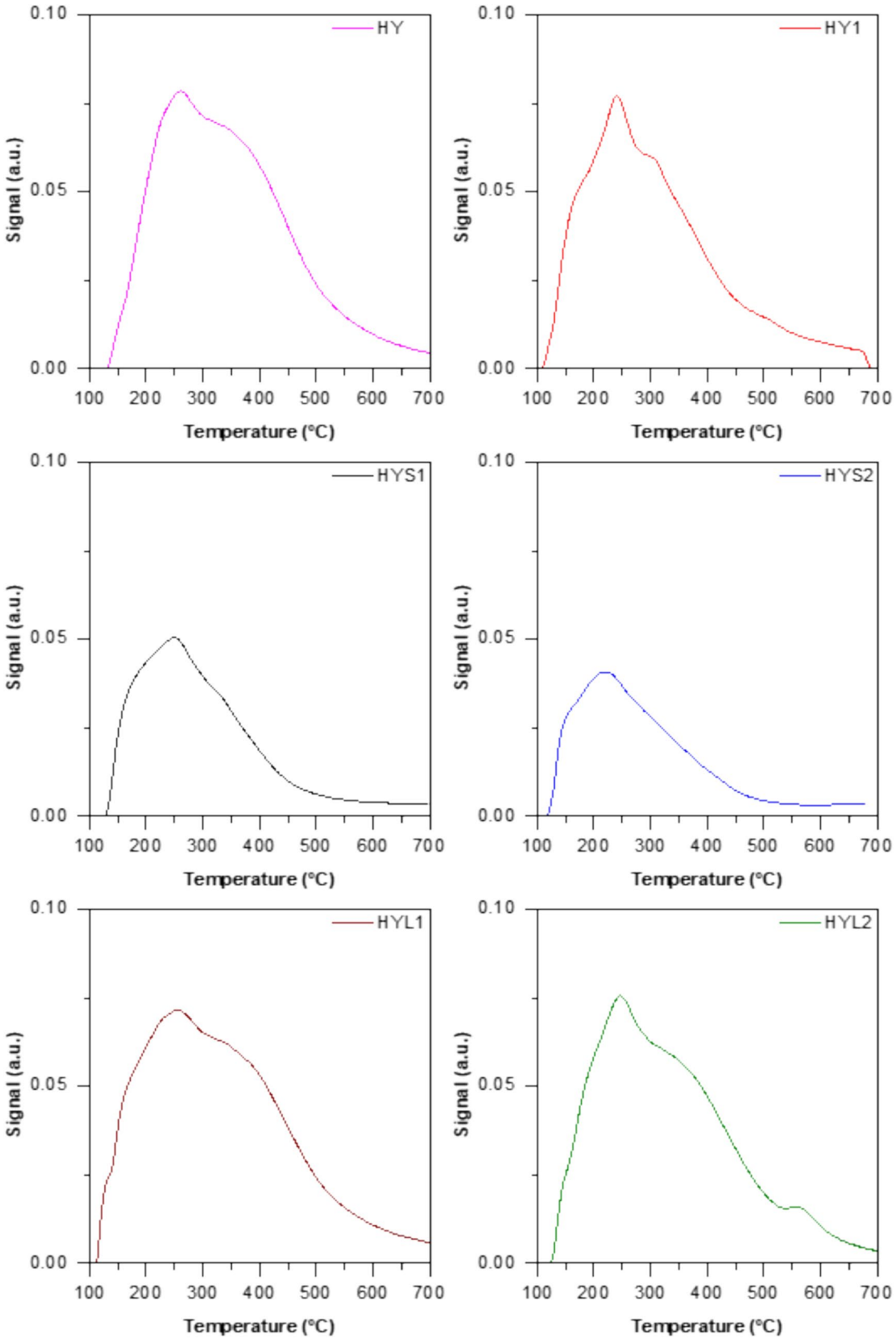

Fig. 7 Ammonia (NH_3-TPD) profiles of Y zeolites

Table 6 Acidity measured by NH_3 and IPam-TPD of nano zeolite Y dealuminated and desilicated

Sample	T(°C)[a]	AS_{peak}[b]	TA[c]	TAn[d]	WS[e]	IS[f]	SS[g]	SS/IS[h]	H^{+i}	S_{micro}/H^{+j}
HY	262	2.83	5.79	1.00	–	0.49	0.51	1.05	1.98	95.50
	405	2.97								
HYS1	180	0.47	2.79	0.48	0.17	0.39	0.45	1.16	2.53	228.64
	250	1.08								
	345	1.25								
HYS2	160	0.24	2.20	0.38	0.11	0.38	0.51	1.32	1.20	358.63
	220	0.84								
	323	1.12								
HYL1	176	0.58	5.10	0.88	0.11	0.43	0.46	1.08	1.25	153.35
	256	2.17								
	396	2.35								
HYL2	178	0.25	5.17	0.89	0.05	0.48	0.47	0.97	1.21	165.43
	247	2.50								
	387	2.42								

[a]Temperature desorption of the different peaks in TPD-NH_3. [b]Amount acid site of different peaks in mmol/g_{cat}. [c]Total acidity by TPD-NH_3 in mmol/g_{cat}. [d]Ratio between acid sites of each sample with the HY zeolite. [e]Fraction of weak acid sites. [f]Fraction of intermediate acid sites. [g]Fraction of strong acid sites. [h]Ratio between strong to intermediate acid sites. [i]Brønsted Acid sites calculated by TPD-IPam in mmol/g_{cat}. [j]Ratio between S_{micro} with Brønsted Acid sites

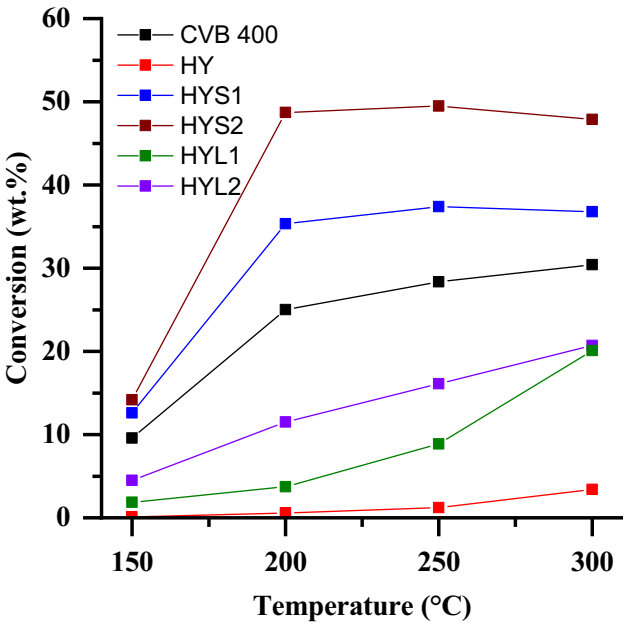

Fig. 8 Effect of temperature on catalytic conversion

medium-sized hydrocarbon fractions. On the contrary, the formation of longer hydrocarbon chains is not favored, possibly due to the insufficient availability of macroporous to facilitate the diffusion of larger molecules and a distribution of acid sites that encourages the union of longer hydrocarbon chains.

Table 7 presents the average conversion and selectivity in the oligomerization of propylene between 200–300 °C. When analyzing dealuminated zeolites, a clear relationship between the average conversion and the Si/Al ratio has been observed. It has been determined that a higher bulk Si/Al ratio and a lower surface Si/Al ratio are linked to higher conversion in propylene oligomerization (Figure S3). This relationship is explained by considering the effects of the bulk and surface Si/Al ratio of the zeolite. A higher bulk Si/Al ratio could decrease deactivation by coke and increase the stability of the catalyst, while a lower surface Si/Al ratio could increase the density of acid sites available for the reaction. The small amount of acid sites in the bulk could generate an improved distribution and accessibility of the active sites and cause a greater density of acid sites on the surface, thus improving the adsorption and activation of propylene [39].

In the case of nanosized zeolite Y desilicated, a lower Si/Al ratio in both the bulk and the surface correlates with a higher conversion. The desilication process generates more mesoporosity and increases the surface area compared to the original nanosized Y zeolite, thus improving the accessibility to acid sites. Improved porosity also promotes better diffusion of reactants and products, reducing mass transfer limitations. Consequently, desilicated zeolites with a lower Si/Al ratio provide a more favorable environment for propylene oligomerization, leading to a higher conversion percentage.

The data presented in Table 7 demonstrates that the characteristics and composition of the zeolitic catalysts significantly impact the conversion and selectivity in propylene oligomerization. The HYS2 and HYL1 catalysts exhibit superior performance in terms of conversion and selectivity for hydrocarbons in the C_5–C_7 range. This could be attributed to their increased total acidity and a higher ratio of

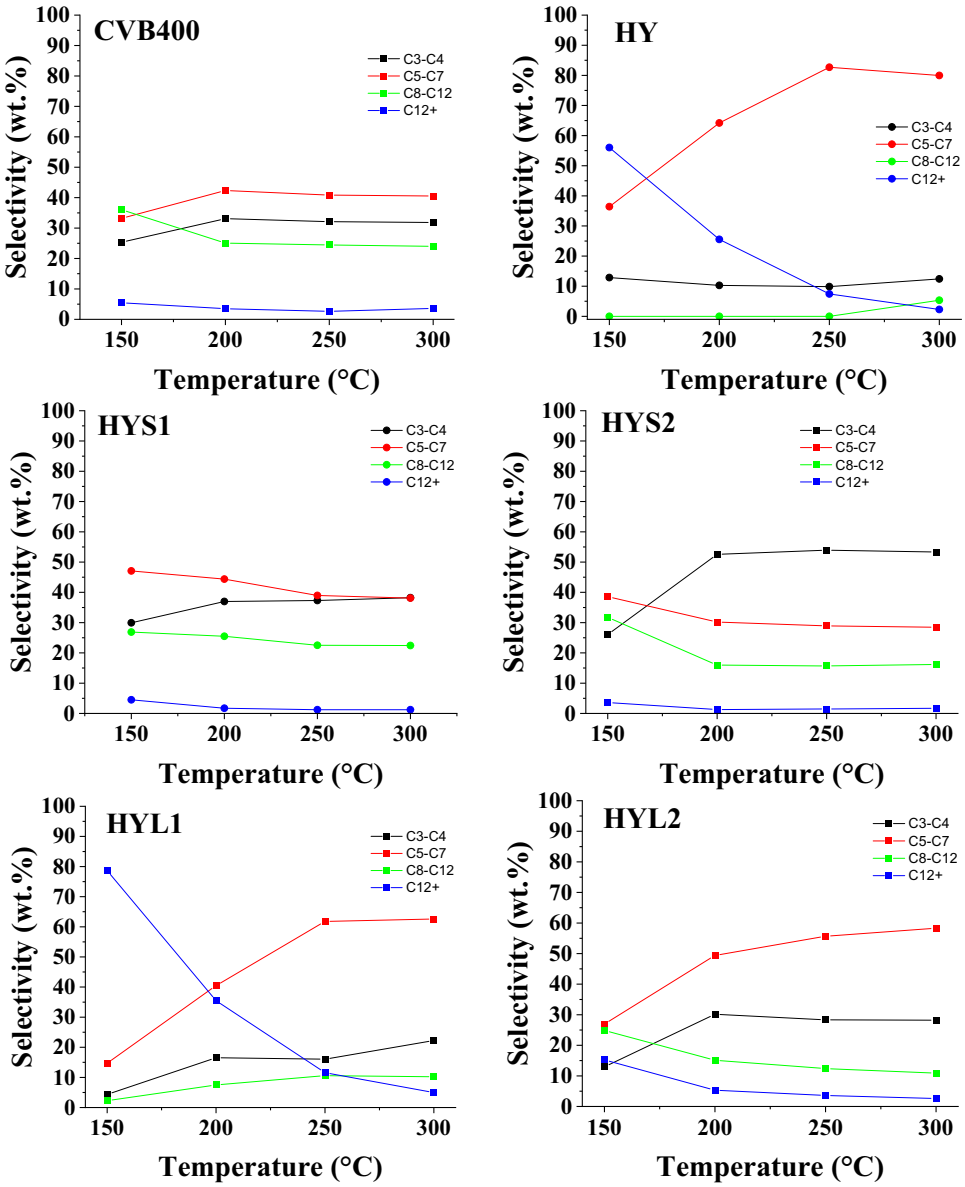

Fig. 9 Effect of temperature on catalytic selectivity

Table 7 Average produced conversion and selectivity in oligomerization between 200–300 °C

Catalyst	Conversion (%)	Selectivity (%)			
		C_3–C_4	C_5–C_7	C_8–C_{12}	C_{12}^+
CVB 400	26.6	34.35	41.25	21.16	3.24
HY	1.74	10.85	75.61	1.78	11.76
HYS1	30.53	37.51	40.48	23.47	1.39
HYS2	36.46	53.27	29.20	15.95	1.49
HYL1	10.90	14.91	45.24	7.58	32.27
HYL2	16.10	28.90	54.46	12.80	3.84

micropore area to Brønsted acid sites. The presence of a significant total acidity indicates a greater number of active sites that can facilitate the reaction, leading to a greater probability of propylene being adsorbed and activated. In addition, a higher ratio of microporous area to Brønsted acid sites suggests a larger amount of active surface for the reaction, which enhances the diffusion and accessibility of propylene molecules to the active sites, thereby encouraging the production of oligomerized products.

The relationship between conversion and yield for each zeolite-based catalyst was analyzed (Figure S4), providing a comparison of obtained products under the same conversion within the temperature range of 200–300 °C. This analysis allowed for the generation of curves that display the optimal relationship between conversion and yield,

highlighting the performance of each catalyst. As the temperature increased, the yield of all hydrocarbons also increased, indicating a direct correlation between temperature and hydrocarbon yield. This trend remained consistent across all catalysts, with yields increasing in tandem with conversion rates. Notably, all catalysts exhibited a higher yield for C_5–C_7 hydrocarbons, which can be attributed to the optimal cracking range for these compounds. However, the HYS2 catalyst demonstrated a unique behavior by showing a higher yield in C_3–C_4 hydrocarbons. This suggests that the HYS2 catalyst promotes more extensive cracking, leading to the production of lighter hydrocarbons. This behavior can be linked to the specific structural and acidic properties of the HYS2 catalyst, particularly the presence of Brønsted acid sites.

The relationship between conversion and selectivity for each zeolite-based catalyst was analyzed (Figure S5). Selectivity towards C_3–C_4 hydrocarbons increased after the dealumination and desilication processes of the zeolites, with an increase observed in the catalysts based on HY, HYL1, and HYL2 zeolites. Subsequently, this selectivity stabilizes as the conversion process continues. This behavior can be attributed to the reduction of the density of Brønsted acid sites in the dealuminated and desilicated structure, favoring the formation of lighter products due to the decreased capacity of the active sites to induce oligomerization of longer chains. Regarding medium-chain hydrocarbons (C_5–C_7), selectivity also increases after structural modification processes but tends to remain constant after reaching a certain level of conversion. With the dealumination process, a slight decrease in selectivity is observed as the conversion increases. However, with catalysts HYL1 and HYL2, the selectivity towards this range of hydrocarbons increases progressively, although their values remain below those achieved by the unmodified HY zeolite. This can be explained by a more efficient distribution of acid sites, which favors the formation of medium-chain fractions but does not achieve the maximum performance observed in untreated zeolite.

For long hydrocarbons chain (C_8–C_{12}), the selectivity increases slightly with conversion in catalysts such as HYL1, but decreases significantly with HYS1, HYS2, and HYL2. This behavior indicates that, despite the greater accessibility to active sites in catalysts, the pore structure and distribution of acid sites are not ideal for promoting the formation of longer hydrocarbons. In the case of long-chain hydrocarbons (C_{12}^{+}), all catalysts show a similar behavior, where a higher conversion leads to a lower selectivity. This effect may be due to diffusion limitations within the zeolite channels and progressive saturation of the active sites, which prevents the efficient formation of longer chains.

4 Conclusion

The synthesis of nanosized zeolites Y without organic templates, with a high Si/Al ratio and in a short period, was successful. The FAU phase was obtained with high relative crystallinity and a smaller crystal size by changing the temperatures using progressive heating and crystallization periods. The desilication and dealumination treatments permitted the generation of zeolites with mesoporous properties despite their small size. A zeolite with a Si/Al ratio of 10.4 (HYS4) was successfully obtained after four consecutive treatments at 700 °C for three hours each. This material exhibited a reduced main crystal size and a higher crystallinity in comparison to zeolite NaY. The high concentration of NaOH caused structural damage to the nanozeolite during the desilication treatment, yet defined porosity and acidic properties were preserved. Conversely, it was shown that the catalytic activity of propene oligomerization is improved by dealumination process, which activates strong acidic sites. Nevertheless, this treatment significantly degrades the nanosized zeolites Y, resulting in low catalyst yields. Consequently, the optimization of steaming conditions and particle size is essential for attaining favorable results, particularly in the context of improving conversion and selectivity.

5 Conflicts of interests

The authors declare no competing interests.

Supplementary Information The online version contains supplementary material available at https://doi.org/10.1007/s10934-024-01703-8.

Acknowledgements The authors acknowledge the financial support from the University of Antioquia and the Committee for the Development of Research – CODI for the project 2022- 55551. Carlos Mendoza acknowledges to the Escuela Normal Superior Genoveva Diaz Educational Institution for providing the necessary time to complete the article's writing.

Author contributions CM: Investigation, Formal analysis, Writing—original draft, Review and editing, Data curation. TB: Investigation, Experimental work, Formal analysis, Writing—original draft, Data curation. RS: Investigation, Conceptualization, Writing—review and editing. CM: Investigation, Conceptualization, Writing—review and editing AE: Supervision, Resources, Funding acquisition, Conceptualization.

Funding Open Access funding provided by Colombia Consortium.

Data availability No datasets were generated or analysed during the current study.

References

1. A.N. Mlinar, G.B. Baur, G.G. Bong, A. Getsoian, A.T. Bell, Propene oligomerization over Ni-exchanged Na-X zeolites. J. Catal. **296**, 156–164 (2012). https://doi.org/10.1016/j.jcat.2012.09.010
2. X. Li et al., Propene oligomerization to high-quality liquid fuels over Ni/HZSM-5. Fuel **144**, 9–14 (2015). https://doi.org/10.1016/j.fuel.2014.12.005
3. P.P. Dik et al., Hydrocracking of vacuum gas oil over NiMo/zeolite-Al_2O_3: Influence of zeolite properties. Fuel **237**, 178–190 (2019). https://doi.org/10.1016/j.fuel.2018.10.012
4. J. Zhao, G. Wang, L. Qin, H. Li, Y. Chen, B. Liu, Synthesis and catalytic cracking performance of mesoporous zeolite y. Catal. Commun. **73**, 98–102 (2016). https://doi.org/10.1016/j.catcom.2015.10.020
5. K. Zhang, M.L. Ostraat, Innovations in hierarchical zeolite synthesis. Catal. Today **264**, 3–15 (2016). https://doi.org/10.1016/j.cattod.2015.08.012
6. Z. Liu, C. Shi, D. Wu, S. He, B. Ren, A simple method of preparation of high silica zeolite y and its performance in the catalytic cracking of cumene. J. Nanotechnol. (2016). https://doi.org/10.1155/2016/1486107
7. C. Mendoza, C. Manrique, A. Echavarría, Impact of lanthanum ion exchange and steaming dealumination on middle distillate production using nanosized Y zeolite catalysts in hydrocracking reactions. RSC Adv. **14**(37), 26760–26774 (2024). https://doi.org/10.1039/D4RA04664A
8. E. Koohsaryan, M. Anbia, Nanosized and hierarchical zeolites: A short review. Cuihua Xuebao/Chinese J. Catal. **37**(4), 447–467 (2016). https://doi.org/10.1016/S1872-2067(15)61038-5
9. M. Zaarour, B. Dong, I. Naydenova, R. Retoux, S. Mintova, Progress in zeolite synthesis promotes advanced applications. Microporous Mesoporous Mater. **189**, 11–21 (2014)
10. E. Kianfar, Nanozeolites: synthesized, properties, applications. J. Sol–Gel Sci. Technol. **91**(2), 415–429 (2019). https://doi.org/10.1007/s10971-019-05012-4
11. T. Derbe, S. Temesgen, M. Bitew, A short review on synthesis, characterization, and applications of zeolites. Adv. Mater. Sci. Eng. **2021**, 1–17 (2021). https://doi.org/10.1155/2021/6637898
12. D. Reinoso, M. Adrover, M. Pedernera, Green synthesis of nanocrystalline faujasite zeolite. Ultrason. Sonochem. **42**, 303–309 (2018). https://doi.org/10.1016/j.ultsonch.2017.11.034
13. P.S. Kuznetsov et al., Synthesis of highly active nanozeolites using methods of mechanical milling, recrystallization, and dealumination (A Review). Pet. Chem. **61**(6), 649–662 (2021). https://doi.org/10.1134/S0965544121050182
14. L.R. Oviedo, V.R. Oviedo, L.D. Dalla Nora, W.L. da Silva, Adsorption of organic dyes onto nanozeolites a machine learning study. Sep. Purif. Technol. **315**, 123712 (2023). https://doi.org/10.1016/j.seppur.2023.123712
15. R.B. Benarmas, A. Bengueddach, F. Di Renzo, Effectiveness of the tetramethylammonium size-modifier in the synthesis of faujasite nanocrystals. Catal. Today **227**, 33–36 (2014). https://doi.org/10.1016/j.cattod.2013.11.007
16. Y.C. Kim, J.Y. Jeong, J.Y. Hwang, S.D. Kim, W.J. Kim, Influencing factors on rapid crystallization of high silica nano-sized zeolite Y without organic template under atmospheric pressure. J. Porous Mater. **16**(3), 299–306 (2009). https://doi.org/10.1007/s10934-008-9200-4
17. D. Karami, S. Rohani, The effect of particle-size reduction of zeolite y on catalytic cracking of bulky hydrocarbons. Pet. Sci. Technol. **31**(16), 1625–1632 (2013). https://doi.org/10.1080/10916466.2010.551231
18. E.E. Freeman, J.J. Neeway, R.K. Motkuri, J.D. Rimer, G. Mpourmpakis, Understanding initial zeolite oligomerization steps with first principles calculations. AIChE J. (2020). https://doi.org/10.1002/aic.17107
19. C. Manrique, R. Solano, C. Mendoza, S. Amaya, A. Echavarría, Hierarchical submicrosized Y zeolites prepared by sequential desilication–dealumination post-synthesis modification and their catalytic performance in vacuum gas oil hydrocracking. New J. Chem. **48**(14), 6188–6200 (2024). https://doi.org/10.1039/D3NJ05551E
20. E. Tabor, M. Bernauer, B. Wichterlová, J. Dedecek, Enhancement of propene oligomerization and aromatization by proximate protons in zeolites; FTIR study of the reaction pathway in ZSM-5. Catal. Sci. Technol. **9**(16), 4262–4275 (2019). https://doi.org/10.1039/C9CY00929A
21. S. Moon, H.-J. Chae, M.B. Park, Oligomerization of light olefins over ZSM-5 and beta zeolite catalysts by modifying textural properties. Appl. Catal. A Gen. **553**, 15–23 (2018). https://doi.org/10.1016/j.apcata.2018.01.015
22. H.O. Mohamed et al., Highly productive framework bounded Ni2+ on hierarchical zeolite for ethylene oligomerization. Chem. Eng. J. **475**, 146077 (2023). https://doi.org/10.1016/j.cej.2023.146077
23. V. Hulea, M. Lallemand, A. Finiels, F. Fajula, Catalytic oligomerization of ethylene over Ni-containing MCM-22, MCM-41 and USY. Stud. Surf. Sci. Catal. **158**, 1621–1628 (2005). https://doi.org/10.1016/s0167-2991(05)80518-x
24. J.W. Yoon, S.H. Jhung, D.H. Choo, S.J. Lee, K.Y. Lee, J.S. Chang, Oligomerization of isobutene over dealuminated Y zeolite catalysts. Appl. Catal. A **337**(1), 73–77 (2008). https://doi.org/10.1016/j.apcata.2007.12.001
25. B. Nkosi, F.T.T. Ng, G.L. Rempel, The oligomerization of butenes with partially alkali exchanged NiNaY zeolite catalysts. Appl. Catal. A **158**(1–2), 225–241 (1997). https://doi.org/10.1016/S0926-860X(96)00420-6
26. R. Dutartre, L.C. De Ménorval, F. Di Renzo, D. McQueen, F. Fajula, P. Schulz, Mesopore formation during steam dealumination of zeolites: Influence of initial aluminum content and crystal size. Microporous Mater. **6**(5–6), 311–320 (1996). https://doi.org/10.1016/0927-6513(96)00039-9
27. A.A. Asadi, S.M. Alavi, S.J. Royaee, M. Bazmi, Dependency of acidic and surficial characteristics of steamed Y zeolite on potentially effective synthesis parameters: Screening, prioritizing and model development. Microporous Mesoporous Mater. **259**, 142–154 (2018). https://doi.org/10.1016/j.micromeso.2017.09.028
28. C. Mendoza, A. Echavarría, A systematic study on the synthesis of nanosized Y zeolite without using organic structure-directing agents: control of Si/Al ratio. J. Porous Mater. **29**(3), 907–919 (2022). https://doi.org/10.1007/s10934-022-01218-0
29. "ASTM D3906–03, Standard test method for determination of relative x-ray diffraction intensities of faujasite-type zeolite containing materials, ASTM International, West Conshohocken, PA, 2008.," https://doi.org/10.1520/D3906-03R13.
30. Zeolite Molecular Sieves: Structure, Chemistry, and Use D. W. Breck (1975). (Union Carbide Corporation, Tarrytown, New

York) John Wiley and Sons, New York, London, Sydney, and Toronto. 1974. 771 pp. $11.95, J. Chromatogr. Sci., vol. 13, no. 4, pp. 18A-18A, https://doi.org/10.1093/chromsci/13.4.18A-c.
31. A. Le Bail, H. Duroy, J.L. Fourquet, Ab-initio structure determination of LiSbWO6 by X-ray powder diffraction. Mater. Res. Bull. **23**(3), 447–452 (1988). https://doi.org/10.1016/0025-5408(88)90019-0
32. Z. Asgar Pour, Y.A. Alassmy, K.O. Sebakhy, A survey on zeolite synthesis and the crystallization process: mechanism of nucleation and growth steps. Crystals **13**(6), 959 (2023). https://doi.org/10.3390/cryst13060959
33. C.J. Mendoza Merlano, T.A. Zepeda, G. Alonso-Nuñez, J.N. Diaz de Leon, C. Manrique, A. Echavarría Isaza, Effect of crystal size on the acidity of nanometric Y zeolite: number of sites, strength, acid nature, and dehydration of 2-propanol. New J. Chem. **46**(30), 14543–14556 (2022). https://doi.org/10.1039/D2NJ01530G
34. Q. Cui et al., Synthesis and characterization of Zr incorporated small crystal size Y zeolite supported NiW catalysts for hydrocracking of vacuum gas oil. Fuel **237**, 597–605 (2019). https://doi.org/10.1016/j.fuel.2018.10.040
35. X. Jia, W. Khan, Z. Wu, J. Choi, A.C.K. Yip, Modern synthesis strategies for hierarchical zeolites: Bottom-up versus top-down strategies. Adv. Powder Technol. **30**(3), 467–484 (2019). https://doi.org/10.1016/j.apt.2018.12.014
36. K. Khivantsev, N.R. Jaegers, L. Kovarik, M.A. Derewinski, J.-H. Kwak, J. Szanyi, On the Nature of Extra-Framework Aluminum Species and Improved Catalytic Properties in Steamed Zeolites. Molecules **27**(7), 2352 (2022). https://doi.org/10.3390/molecules27072352
37. L. Shi et al., Creating intraparticle mesopores inside ZSM-5 nanocrystals under OSDA-free conditions and achievement of high activity in LDPE degradation. Microporous Mesoporous Mater. **258**, 178–188 (2018). https://doi.org/10.1016/j.micromeso.2017.09.019
38. D.S. Oliveira, R.B. Lima, S.B.C. Pergher, V.P.S. Caldeira, Hierarchical Zeolite Synthesis by Alkaline Treatment: Advantages and Applications. Catalysts **13**(2), 316 (2023). https://doi.org/10.3390/catal13020316
39. V. Verdoliva, M. Saviano, S. De Luca, Zeolites as acid/basic solid catalysts: recent synthetic developments. Catalysts **9**(3), 248 (2019). https://doi.org/10.3390/catal9030248